Howard Hughes Medical Institute

Published as: *Science*. 2018 February 23; 359(6378): 940–944.

Structures of human PRC2 with its cofactors AEBP2 and JARID2

Vignesh Kasinath[1,2], **Marco Faini**[3,*], **Simon Poepsel**[1,2,*], **Dvir Reif**[1], **Xinyu Ashlee Feng**[4], **Goran Stjepanovic**[1,2], **Ruedi Aebersold**[3,5], and **Eva Nogales**[1,2,6,†]

[1]QB3 Institute, Department of Molecular and Cell Biology, University of California, Berkeley, CA 94720, USA [2]Molecular Biophysics and Integrated Bioimaging Division, Lawrence Berkeley National Laboratory, Berkeley, CA 94720, USA [3]Department of Biology, Institute of Molecular Systems Biology, ETH Zurich, 8093 Zurich, Switzerland [4]Department of Chemistry, University of California, Berkeley, CA 94720, USA [5]Faculty of Science, University of Zurich, Zurich, Switzerland [6]Howard Hughes Medical Institute, University of California, Berkeley, CA 94720, USA

Abstract

Transcriptionally repressive histone H3 lysine 27 methylation by Polycomb repressive complex 2 (PRC2) is essential for cellular differentiation and development. Here we report cryo–electron microscopy structures of human PRC2 in a basal state and two distinct active states while in complex with its cofactors JARID2 and AEBP2. Both cofactors mimic the binding of histone H3 tails. JARID2, methylated by PRC2, mimics a methylated H3 tail to stimulate PRC2 activity, whereas AEBP2 interacts with the RBAP48 subunit, mimicking an unmodified H3 tail. SUZ12 interacts with all other subunits within the assembly and thus contributes to the stability of the complex. Our analysis defines the complete architecture of a functionally relevant PRC2 and provides a structural framework to understand its regulation by cofactors, histone tails, and RNA.

Polycomb repressive complex 2 (PRC2) is responsible for introducing and maintaining heterochromatin regions and for spreading a transcriptionally repressive state locally (1, 2).

---

†Corresponding author: enogales@lbl.gov.
*These authors contributed equally to this work.

Author contributions: V.K. established experimental procedures, expressed and purified the different complexes, prepared the sample and cryo-grids, collected and processed all EM data, and carried out model building and refinement. D.R. and X.A.F. assisted with molecular cloning, protein purification, and negative-stain EM sample screening. S.P. gave input and contributed to discussions during the course of the work and provided critical feedback during manuscript preparation. M.F. and R.A. performed the mass spectrometry experiments. M.F. analyzed the targeted MS data. V.K. and M.F. analyzed the XL-MS data. V.K. and G.S. performed the hydrogen-deuterium exchange experiments and analyzed the data. V.K. and E.N. analyzed all the data. E.N. and R.A. supervised the work. V.K. and E.N. wrote the manuscript with input from all authors.

Data and materials availability: Cryo-EM density maps and fitted models have been deposited in the Electron Microscopy Data Bank (EMDB) and the PDB for the complete PRC2-AJ$_{106}$ compact active state (EMD-7334 and PDB 6C23), PRC2-AJ$_{106}$ extended active state (EMD-7335 and PDB 6C24), and PRC2-AJ$_{119}$ (EMD-7337). All the primary MS data are available through the PRIDE archive and can be accessed via ProteomeXchange (ID, PXD008605).

SUPPLEMENTARY MATERIALS
www.sciencemag.org/content/359/6378/940/suppl/DC1
Materials and Methods
Figs. S1 to S10
Table S1
References (30–54)
Movie S1

PRC2 consists of four core proteins: EZH2, EED, SUZ12, and RBAP46/RBAP48 (3). EZH2 catalyzes the trimethylation of histone H3 at lysine 27 (H3K27me3), a repressive marker ultimately resulting in transcriptional silencing through chromatin compaction (1). EED binding of H3K27me3 allosterically activates EZH2 (4, 5). PRC2 associates with several cofactors that may modulate its activity and aid in its recruitment to chromatin (3, 6–9). The best characterized cofactors are AEBP2 and JARID2, which coexist in PRC2 complexes (6, 10, 11).

A structure of human PRC2 with AEBP2, obtained using negative-stain electron microscopy (EM), elucidated the overall architecture and subunit organization of the complex (12). More recently, crystal structures of the catalytic lobe—consisting of EZH2, EED, and the VEFS domain of SUZ12 (refer to Fig. 1A for proteins and domains), with either trimethylated H3 or a trimethylated JARID2 peptide bound to EED—hinted at a potential mechanism for allosteric activation of EZH2 (4, 5, 13–15). The binding of methylated JARID2 to EED, mimicking that of a methylated histone H3 tail, has been suggested to play an important role in promoting PRC2 methyltransferase activity toward nucleosomes in the absence of preexisting H3K27me3 (14). In both cases, binding of the methylated peptide stabilized a stimulatory responsive motif (SRM) that is otherwise disordered and that subsequently interacts with the catalytic SET domain in EZH2 (4, 13, 15). Additionally, the crystal structure of RBAP48 bound to a histone peptide described RBAP48's preference for unmodified H3 over H3K4me3, which is known to inhibit PRC2 activity (16). However, the mechanisms by which different histone substrates and cofactors regulate the activity of the complete complex are unknown. Given that cofactors are thought to be integral parts of PRC2 complexes in vivo (10, 17–19), how they affect PRC2 structure and function remains a crucially important question.

Here we report three high-resolution cryo-EM structures of the complete human PRC2 with the cofactors AEBP2 and JARID2, respectively corresponding to two distinct active states and a basal state in which PRC2 is bound to AEBP2 and a shorter JARID2 construct. The structures show that both JARID2 and AEBP2 mimic histone tails binding to PRC2 and that SUZ12 interacts with all other subunits and the cofactors. SUZ12 and AEBP2, with the help of JARID2, bridge the catalytic lobe with the rest of PRC2 and play a pivotal role in maintaining its structural integrity. Collectively, these structures elucidate the synergistic effect of AEBP2 and JARID2 on PRC2 activity.

To maximize the resolution of our cryo-EM analysis, we purified PRC2 with truncations in the core subunits EED and SUZ12 to eliminate large unstructured regions without a known functional role (methods). We also used a minimal construct of JARID2 (amino acid residues 106 to 450) that has been shown to be sufficient for binding nucleosomes and stimulating PRC2 activity (6, 7, 18). We refer to this 330-kDa complex as PRC2-AJ$_{106}$. Cross-linking mass spectrometry (XL-MS) (Fig. 1B) and cryo-EM studies (fig. S1A) both confirmed that the truncations did not affect the overall architecture of the complex. JARID2 has been shown to be a substrate of PRC2 and to bind to EED when methylated at K116 (13, 14). We obtained reconstructions at 3.5 and 3.9 Å for two coexisting conformational states of PRC2-AJ$_{106}$ (Fig. 1C and figs. S1B and S2), both containing a substrate JARID2 at the EZH2 active site, as well as a stimulatory, methylated JARID2 bound to EED (Fig. 2, A and

B; fig. S3; and table S1). Therefore, we consider both states to be active and refer to them as "compact active" and "extended active" states, respectively. Although there is no significant difference in the conformation of the catalytic SET domain (fig. S4, A and B), the two states differ in the conformations of the SRM, which is stably bound in the compact active state but disordered in the extended active state, and of the SBD-SANT1 module, where SBD stands for SANT1-binding domain. Whereas in the compact active state, the SBD is bent and the SANT1 is packed against the SBD, in the extended active state, the SBD is straight and the SBD-SANT1 module stands tall over the EED (Fig. 1C).

Figure 1D shows the overall structure of PRC2 in the compact active state, bound to its two cofactors. Adding to the previous description of the catalytic half comprising the top lobe, which includes EZH2, EED, and the SUZ12 VEFS domain, our study now describes the bottom lobe that includes the rest of SUZ12, RBAP48, and stably bound segments of AEBP2 and JARID2. The resolution of our cryo-EM structures, together with XL-MS data, allowed us to generate an atomic model of this complete, functionally relevant, six-subunit human complex (movie S1).

The previous crystal structure of the human catalytic subcomplex containing an activating peptide bound to EED corresponds closely to the compact active state described here (4, 13), likely because the crystal structure was trapped in the more compact state. In our study, the JARID2 segment bound to EED has fewer interactions with the SRM in the extended active state (Fig. 2A). In the compact active state, the interactions of methylated JARID2 with the EED aromatic cage (F97, Y148, and Y365) and the side chain of D136 from the EZH2 SRM are consistent with those previously reported (Fig. 2A) (13). To probe further the role of JARID2 K116me2/3 in the conformational partitioning of PRC2, we also visualized a ternary complex of PRC2 bound to AEBP2 and a shorter JARID2 construct (residues 119 to 450) lacking K116, which we refer to as PRC2-AJ$_{119}$ (fig. S5). As expected, there is no JARID2 bound to either EED or the EZH2 active site (Fig. 2C), further supporting our assignments of the JARID2 segments in these regions for the active states of PRC2-AJ$_{106}$. The PRC2-AJ$_{119}$ structure overall resembles the extended active state (i.e., disordered SRM and straight SBD) but differs from it in the relative position of the methyltransferase catalytic SET domain with respect to EED (fig. S4, B and C). Thus, the absence of JARID2 residues 106 to 118 results in a PRC2 structure that lacks the conformational landmarks associated with activation, and we refer to the structure of PRC2-AJ$_{119}$ as the extended basal state.

Our PRC2 structures validate biochemical experiments demonstrating that JARID2 is a substrate of PRC2 (14) through the direct visualization of two JARID2 molecules simultaneously bound to the allosteric and active sites of the complex. Such structures lend strong support to a model in which PRC2 initially acts on un-methylated JARID2 and methylates it at K116, and this methylated JARID2 then binds EED, resulting in allosteric stimulation of PRC2 and a cascade of PRC2 activity toward additional un-methylated JARID2 substrate. Additionally, our observations emphasize the conformational versatility of PRC2, wherein the binding of a methylated peptide to EED is not strictly coupled to EZH2 (SRM) stabilization. The existence of two distinct active PRC2 states suggest that additional signals could exploit the conformational complexity of PRC2 to fine-tune PRC2

methyltransferase activity, its interaction with nucleosomes, and/or other functional aspects of the complex. Furthermore, although we observed density for both cofactors in our structure (discussed below), both AEBP2 and JARID2 contain large disordered regions that are unresolved in our reconstructions. This flexibility of the cofactors, together with the coexistence of multiple conformational states, further reflects the intrinsic conformational variability that may be exploited to integrate diverse cues critical for the complex regulation of PRC2 in different biological contexts.

Our MS analysis of PRC2-AJ_{106} revealed JARID2 to be mono-, di-, and trimethylated at K116 and phosphorylated on neighboring serine residues (S120, S124, or S126) (fig. S3, A and B). A similar MS analysis of PRC2-AJ_{119} showed no differences in the phosphorylation of these residues in JARID2 (fig. S3B), suggesting that JARID2 K116 methylation by PRC2 is unlikely to be required for this phosphorylation. It is possible that phosphorylation facilitates processivity of JARID2 methylation by PRC2, perhaps by decreasing the off rate of the K116me1 peptide at the active site. It is tempting to speculate that JARID2 phosphorylation could be part of a mechanism of controlling PRC2 methyltransferase activity toward JARID2 and, thus, its activity toward other targets as well. Further studies aimed at elucidating the relationship between serine phosphorylation and different methylation states of JARID2, as well as the conformational states of PRC2, hold promise for enhancing our mechanistic understanding of PRC2 regulation and function.

AEBP2, like JARID2, plays a role in the stimulation of PRC2 methyltransferase activity (17, 20), but the structural basis for such stimulation is unknown. AEBP2 contains three C2H2-type zinc fingers (17), and previous labeling studies localized these domains by the top lobe of PRC2 near the EED and EZH2 (SET) domains (12). In our cryo-EM reconstructions, the N-terminal region of AEBP2 containing the three zinc fingers is disordered, whereas part of the C-terminal region is clearly visible and appears to have a stabilizing effect on the complex (Fig. 2D and fig. S6A). The fold of AEBP2 is mostly dictated by its interactions with SUZ12. Residues 269 to 283 of AEBP2 interact with the “foot” of the complex, which is part of SUZ12 (Fig. 2D; discussed below), and a preceding helical segment (residues 246 to 266) forms extensive hydrophobic interactions with a helix near the N terminus of SUZ12 (referred to as ABH in Figs. 1D and 2D and fig. S7A). Most importantly, our structures reveal that K294 and R295, at the C terminus of AEBP2, mimic the binding of R2 and K4 of histone H3 to RBAP48 (16) (Fig. 2, D to F). This finding suggests a potential interplay between AEBP2 and unmodified H3K4 when PRC2 is recruited to nucleosomes.

Although unmodified H3K4 has been proposed to stimulate PRC2 through its binding to RBAP48 (16), a functional explanation for this allosteric effect has been hard to envision, especially because RBAP48 is located 60 Å away from the EZH2 SET domain (fig. S6B). Our structures now suggest that the interactions of the C-terminal region of AEBP2 with RBAP48 and SUZ12 help position the more flexible N-terminal elements of AEBP2, including the three zinc fingers, near the EZH2 SET domain (fig. S6C). This proposal is supported by our XL-MS analysis, which shows that the region comprising residues 160 to 200 of AEBP2, which is rich in lysine and arginine, extends toward and likely interacts with the SET domain (fig. S6, A and C). Thus, AEBP2 appears to have the potential to establish a

structural bridge between RBAP48 and the SET domain, which we propose contributes to the allosteric coupling of these distant sites (fig. S6C and S7C).

Our work directly shows that both cofactors, AEBP2 and JARID2, contain segments that simultaneously engage histone tail binding sites on PRC2. The observation that both cofactors mimic histone H3 tails suggests that they could function to regulate PRC2 activity in diverse chromatin environments by selectively overriding the effects of existing histone marks. JARID2 K116me2/3 can dispense with the need for H3K27me3 to stimulate PRC2, and AEBP2 interacts with RBAP48 at a site that is engaged by unmethylated H3K4, but not by the inhibitory H3K4me3 (16), potentially allowing PRC2 to remain active even in the presence of the H3K4me3 mark.

Structural and functional information about the role played by SUZ12 has so far been limited to the C-terminal VEFS domain (4, 13, 15, 20). Our structures now show that SUZ12 is critical for maintaining the integrity of the full complex and for the synergistic effect of AEBP2 and JARID2 on PRC2 activity. SUZ12 follows a complicated path through the complex and interacts with all other core components, as well as the two cofactors (Fig. 3A and fig. S8A). SUZ12 contains a C2H2-type zinc-finger domain (residues 448 to 472) (20) (Fig. 3D) that provides a platform for the folding of regions extending both N- and C-terminally (residues 426 to 548), which we collectively refer to as the “neck” region (NR in Fig. 3, A and B, and fig. S8A). The SUZ12 neck region interacts both with an AEBP2 helical segment (residues 246 to 266) and a lysine- and arginine-rich region of AEBP2 (residues 160 to 200) and thereby helps AEBP2 establish a bridge between RBAP48 and the EZH2 SET domain. (Fig. 3B and 4C and fig. S6C). In addition, the SUZ12 neck region forms extensive hydrophobic interactions with catalytically important regions of EZH2 (the so-called SAL motif), EED, and the SUZ12 VEFS domain. Mutations in residues of the SUZ12 neck region (R508C) and SUZ12 VEFS (N562S) seen in adenocarcinoma and myeloproliferative neoplasms (21, 22) map to the contacts with the EZH2 (SAL) and SUZ12 neck region, respectively. Although the VEFS domain of SUZ12 has been known to be important for the proper folding and activity of EZH2 (4, 16), we find additionally that the interaction of the SUZ12 neck region with the VEFS domain is important for the stability of SUZ12 within the PRC2 complex (Fig. 3E). We also find that the region of SUZ12 corresponding to residues 109 to 136 wraps around RBAP48 in a manner similar to the folding of EZH2 around EED and is solely responsible for the incorporation of RBAP48 in the PRC2 complex (4, 13, 15) (fig. S7B).

The SUZ12 neck region serves as a scaffold for interaction with both cofactors. In addition to its critical role in the folding of AEBP2, as described above, the SUZ12 neck is also the region of stable interaction with JARID2 (Fig. 4). Previous studies showed that a JARID2 construct containing residues 147 to 165 is important for interaction with SUZ12 (19). Comparison of our structure of PRC2-AJ_{106} with a 4.6-Å-resolution cryo-EM structure of PRC2-AEBP2 (i.e., lacking JARID2) (23) shows the presence of an additional density in the vicinity of the SUZ12 zinc-finger domain that we assigned to a JARID2 segment corresponding to residues 140 to 166 (Fig. 4, A and B). This assignment agrees with our XL-MS data, which show the presence of cross-links between this region of JARID2 and the SUZ12 zinc-finger domain within the neck region (Fig. 4C). The JARID2 segment forms a

helix-turn-helix motif that wedges in between AEBP2 and a β-sheet region within the SUZ12 neck (Fig. 4D). The three-way junction between SUZ12, AEBP2, and JARID2 is important for stability: A core PRC2 complex in the absence of JARID2 and AEBP2 becomes dramatically more flexible, and its overall stability is decreased (Fig. 4D) (12). Our structures show how JARID2 stabilizes the interaction between AEBP2 and SUZ12 to maintain the integrity of the complex by stapling the top, catalytic, and bottom lobes together (Fig. 1D and 4D).

Last, we observed a SUZ12 domain that is rich in β-sheet structure forming the "foot" of the complex [β-sheet domain (BSD) in Fig. 3C and fig. S8, A and B]. Because of its flexibility (fig. S2), we were only able to build this region as a polyalanine chain (Fig. 3C). A domain search across the Protein Data Bank (PDB) indicated that it resembles an RNA recognition motif (RRM)–like fold (24) (fig. S7B). SUZ12 and EZH2 have been implicated in RNA binding (25–27). Long non-coding RNAs (lncRNAs) have been proposed to play a role in PRC2 recruitment to nucleosomes (28) or to affect its activity on nucleosome substrates (29). We carried out hydrogen-deuterium exchange experiments in the presence and absence of the lncRNA XIST A-repeat that showed that this domain contributes to RNA binding (fig. S8, C and D). Additional roles, such as binding to nucleosomes or DNA, are also conceivable for the flexible, RRM-like β-sheet–rich domain located at the foot of the complex.

Our structures of the full human PRC2 in complex with the two critical cofactors AEBP2 and JARID2 include regions of AEBP2, JARID2, and SUZ12 for which there was no prior structural information (fig. S9). Whereas the catalytic lobe of PRC2 containing EZH2, EED, and part of SUZ12 has been shown to be sufficient for methyltransferase activity, the bottom lobe of PRC2 described here is likely to provide additional regulatory functions for the activity and recruitment of the complex. Our structures highlight the critical role played by SUZ12 in maintaining the integrity of the full complex. The interactions of cofactors AEBP2 and JARID2 with PRC2, mimicking those of histone H3 tails, result in two active states and not only contribute to the global stabilization of PRC2 (fig. S9), but also potentially aid in the synergistic stimulation of PRC2 activity and regulated recruitment to chromatin.

Supplementary Material

Refer to Web version on PubMed Central for supplementary material.

Acknowledgments

We thank D. Toso (Bay Area Cryo-EM consortium) and C. Hong, R. Huang, and Z. Yu (Janelia CryoEM Facility) for help with microscope operation and data collection; P. Grob, J. Fang, and Y. Liu for technical support; and T. Houweling, A. Chintangal, and P. Tobias for computer support. We thank R. Danev for his help with the operation of the Volta Phase plate. Computational resources were provided in part by the National Energy Research Scientific Computing Center (DE-AC02-05CH11231) and the LAWRENCIUM computing cluster at Lawrence Berkeley National Laboratory.

Funding: This work was in part funded by Eli Lilly through the Lilly Research Award Program. V.K. was supported by a postdoctoral fellowship from Helen Hay Whitney Foundation. S.P. was supported by the Alexander von Humboldt Foundation (Germany) as a Feodor-Lynen postdoctoral fellow. M.F. was supported by a Long-Term Fellowship from the European Molecular Biology Organization. R.A. was supported by the European Union 7th Framework Program (PROSPECTS, HEALTH-F4-2008-201648), the European Research Council (ERC Advanced

Grants 233226 and 670821), and the Innovative Medicines Initiative Joint Undertaking (ULTRA-DD, grant 115766). E.N. is a Howard Hughes Medical Institute Investigator.

REFERENCES AND NOTES

1. Cao R, et al. Science. 2002; 298:1039–1043. [PubMed: 12351676]
2. Talbert PB, Henikoff S. Nat Rev Genet. 2006; 7:793–803. [PubMed: 16983375]
3. Margueron R, Reinberg D. Nature. 2011; 469:343–349. [PubMed: 21248841]
4. Jiao L, Liu X. Science. 2015; 350:aac4383. [PubMed: 26472914]
5. Margueron R, et al. Nature. 2009; 461:762–767. [PubMed: 19767730]
6. Son J, Shen SS, Margueron R, Reinberg D. Genes Dev. 2013; 27:2663–2677. [PubMed: 24352422]
7. Kaneko S, et al. Mol Cell. 2014; 53:290–300. [PubMed: 24374312]
8. Walker E, et al. Cell Stem Cell. 2010; 6:153–166. [PubMed: 20144788]
9. Zhang Z, et al. Stem Cells. 2011; 29:229–240. [PubMed: 21732481]
10. Grijzenhout A, et al. Development. 2016; 143:2716–2723. [PubMed: 27317809]
11. Hauri S, et al. Cell Rep. 2016; 17:583–595. [PubMed: 27705803]
12. Ciferri C, et al. eLife. 2012; 1:e00005. [PubMed: 23110252]
13. Justin N, et al. Nat Commun. 2016; 7:11316. [PubMed: 27121947]
14. Sanulli S, et al. Mol Cell. 2015; 57:769–783. [PubMed: 25620564]
15. Brooun A, et al. Nat Commun. 2016; 7:11384. [PubMed: 27122193]
16. Schmitges FW, et al. Mol Cell. 2011; 42:330–341. [PubMed: 21549310]
17. Kim H, Kang K, Kim J. Nucleic Acids Res. 2009; 37:2940–2950. [PubMed: 19293275]
18. Li G, et al. Genes Dev. 2010; 24:368–380. [PubMed: 20123894]
19. Pasini D, et al. Nature. 2010; 464:306–310. [PubMed: 20075857]
20. Cao R, Zhang Y. Mol Cell. 2004; 15:57–67. [PubMed: 15225548]
21. Brecqueville M, et al. Blood Cancer J. 2011; 1:e33. [PubMed: 22829192]
22. Mouradov D, et al. Cancer Res. 2014; 74:3238–3247. [PubMed: 24755471]
23. Poepsel S, Kasinath V, Nogales E. Nat Struct Mol Biol. 2018
24. Maris C, Dominguez C, Allain FH. FEBS J. 2005; 272:2118–2131. [PubMed: 15853797]
25. Betancur JG, Tomari Y. RNA Biol. 2015; 12:959–965. [PubMed: 26177152]
26. Kaneko S, et al. Genes Dev. 2010; 24:2615–2620. [PubMed: 21123648]
27. Kanhere A, et al. Mol Cell. 2010; 38:675–688. [PubMed: 20542000]
28. Davidovich C, Cech TR. RNA. 2015; 21:2007–2022. [PubMed: 26574518]
29. Wang X, et al. Nat Struct Mol Biol. 2017; 24:1028–1038. [PubMed: 29058709]

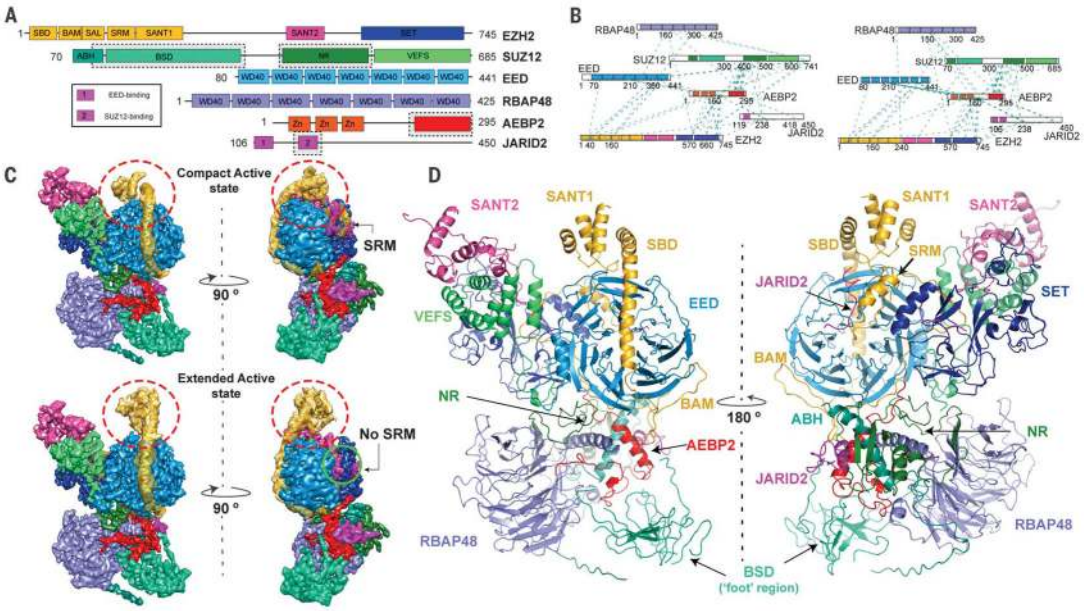

Fig. 1. Cryo-EM structure of PRC2-JARID2-AEBP2

(**A**) Schematic representation of the proteins in the PRC2-JARID2-AEBP2 complex. Dashed boxes highlight regions described in our study for which structural information was previously unavailable. (**B**) XL-MS results for PRC2-AJ$_{119}$ (left) and PRC2-AJ$_{106}$ (right). (**C**) Cryo-EM densities for the two conformational states (compact active and extended active) of PRC2-AJ$_{106}$, with differences in SBD and SANT1 highlighted by the red dashed circles. SRM is ordered and visible only in the compact active state (top). The JARID2 K116me3 fragment is bound in both states. (**D**) Atomic model of the compact active state, with EZH2 (SANT1, SBD, BAM, and SRM) in gold, EZH2 (SET) in dark blue, EZH2 (SANT2) in pink, EED in light blue, RBAP48 in violet, AEBP2 in red, JARID2 in magenta, SUZ12 (ABH and BSD) in mint green, SUZ12 (NR) in dark green, and SUZ12 (VEFS) in bright green. This color-coding also applies to (B) and (C).

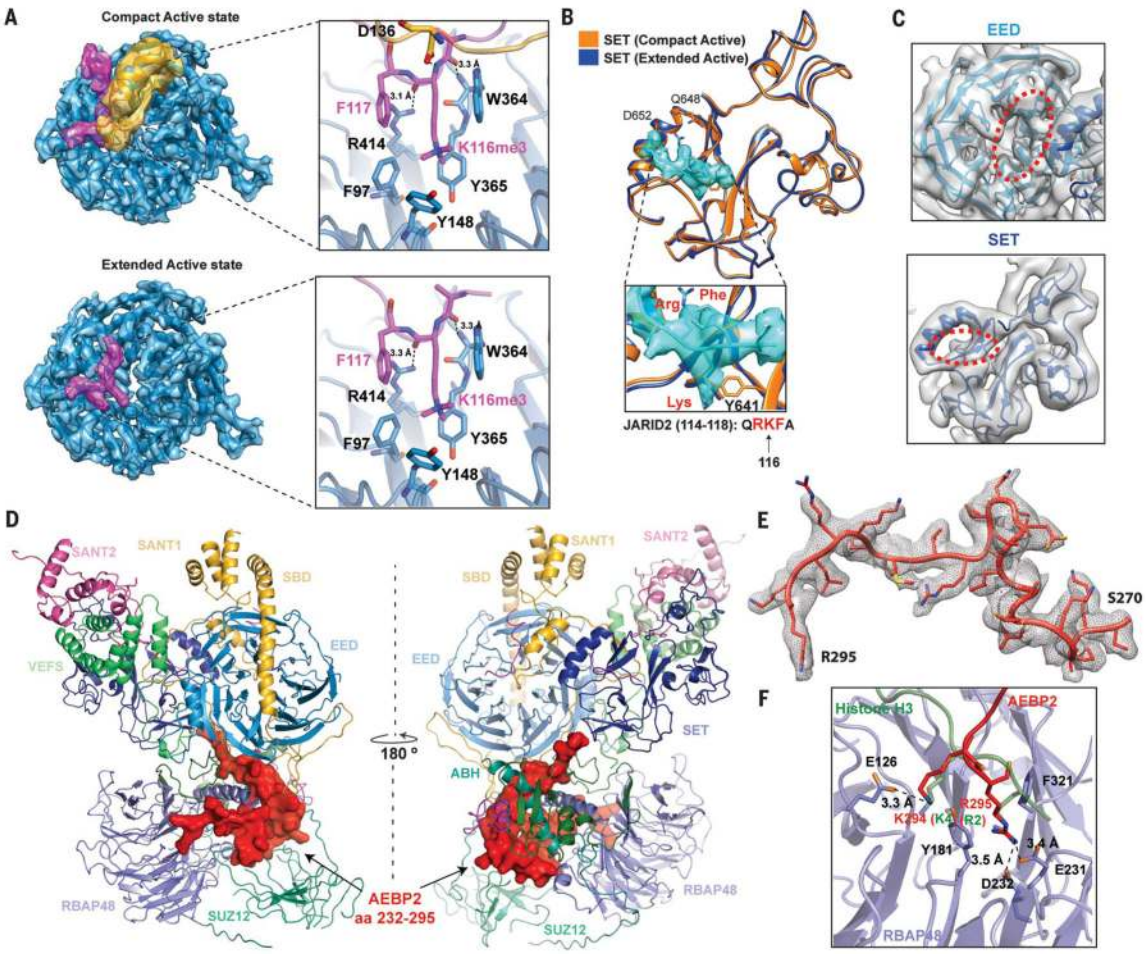

Fig. 2. Cofactors AEBP2 and JARID2 mimic histone H3 tails

(**A**) Interaction of JARID2 K116me3 (magenta) with EED (light blue) in the two conformational states sampled by PRC2-AJ$_{106}$. JARID2 K116me3 sits in the middle of an aromatic cage (F97, Y148, and Y365) with hydrogen-bond interactions (R414:F117 and W364:R115) that stabilize the JARID2 peptide backbone. In the compact active state, additional interaction between EZH2 D136 and the backbone amide of JARID2 K116 helps position the EZH2 SRM helix (gold) next to the EZH2 SETdomain. (**B**) The EZH2 SETdomain of PRC2-AJ$_{106}$ is in a similar conformation in both states (compact active, orange; extended active, blue; Cα root mean square deviation = 0.74 Å; fig. S4B) and is bound to a substrate peptide (cyan). Inset, density of substrate observed in our cryo-EM reconstruction shown with a model for JARID2 residues 114 to 118. (**C**) Cryo-EM density of the PRC2-AJ$_{119}$ EED and EZH2 SETregions with ribbon representations of EED (light blue) and SET (dark blue), showing the absence of both the stimulatory fragment bound to EED and the substrate bound to the SETdomain (red dashed circles). (**D**) AEBP2 (residues 232 to 295, red), shown in surface representation, connects RBAP48, the SUZ12 N-terminal region, and the EZH2 SETdomain. (**E**) Map versus model of the AEBP2 region that binds RBAP48 at the histone H3 binding site. (**F**) View of the RBAP48 WD40 domain showing, in stick representation, the conserved amino acids in RBAP48 (violet) interacting with K294

and R295 of AEBP2 (red). The overlay of the crystal structure of the *Drosophila* homolog of RBAP48 (NURF55) bound to unmodified histone H3 peptide [PDB ID, 2YBA (16); green] highlights the similarity of the binding mode between AEBP2 and histone H3, with all key residues in identical conformations; only the AEBP2 (H3) residues R295 (R2) and K294 (K4) are shown for clarity. Single-letter abbreviations for the amino acid residues are as follows: A, Ala; C, Cys; D, Asp; E, Glu; F, Phe; G, Gly; H, His; I, Ile; K, Lys; L, Leu; M, Met; N, Asn; P, Pro; Q, Gln; R, Arg; S, Ser; T, Thr; V, Val; W, Trp; and Y, Tyr.

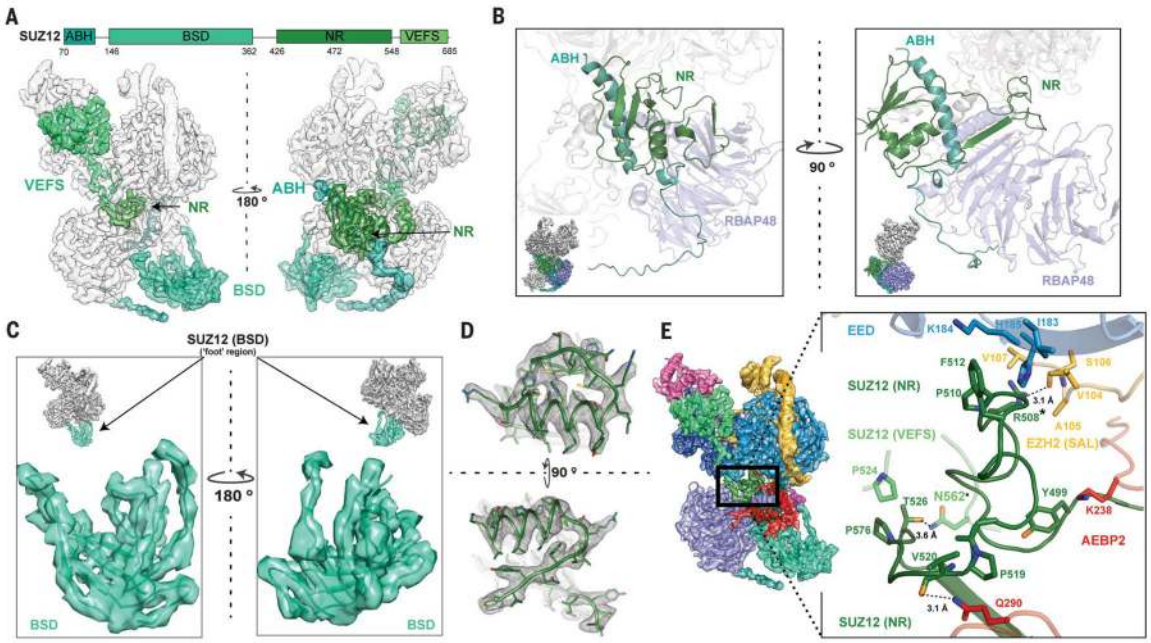

Fig. 3. SUZ12 interacts with all subunits of PRC2

(**A**) Schematic representation of the different domains of SUZ12 (shades of green; top) and cryo-EM density of SUZ12 showing the location of each domain within PRC2 (bottom). (**B**) Orthogonal views of the SUZ12 AEBP2-binding helix (ABH) and neck region (NR), defining the part of SUZ12 at the center of the complex. The insets show the relative location of these regions within the full PRC2 complex. (**C**) Cryo-EM density of the β-sheet–rich domain (BSD) making up the "foot" of the complex, with a fitted polyalanine model. Top insets, position of BSD within PRC2. (**D**) Map versus model for the SUZ12 zinc-finger domain, which interacts with AEBP2 (residues 246 to 266), the helix-turn-helix (HTH) of JARID2 (Fig. 4), and the ABH of SUZ12. (**E**) Close-up of the neck region of PRC2 showing, in stick representation, the amino acids contributing to the hydrophobic interactions between the SUZ12 NR, the SAL of EZH2, EED, and the SUZ12 VEFS. Dotted lines indicate potential hydrogen bonds. Mutations in R508 and N562 (asterisks) have been observed in a number of cancers.

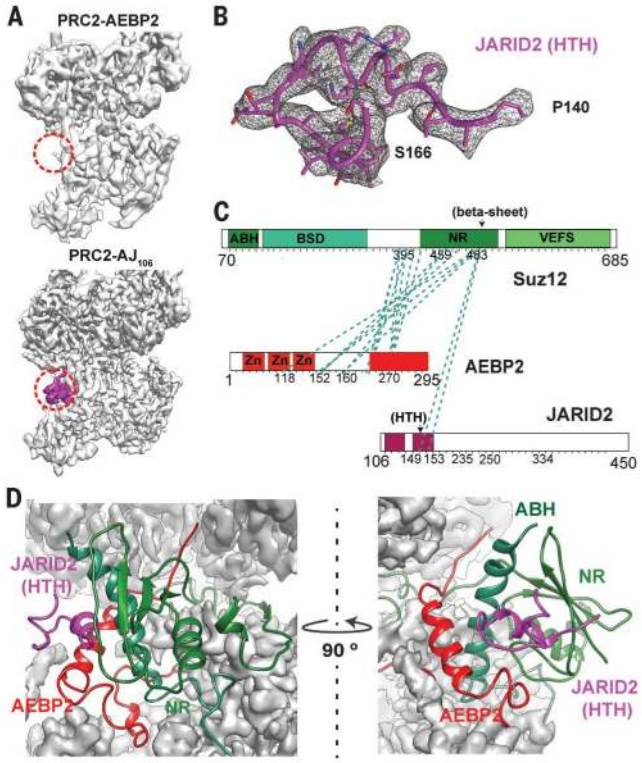

Fig. 4. JARID2-AEBP2-SUZ12 interactions contribute to the stability of PRC2

(**A**) The density region marked by the red dashed circle is only present in JARID2-containing complexes [PRC2-AEBP2 (top) and PRC2-AJ$_{106}$ (bottom, with the JARID2 segment in magenta)]. (**B**) Map versus model for JARID2 residues 140 to 166. The model built into the density agrees well with the HTH secondary structure prediction for this region. (**C**) Cross-links of the SUZ12 NR with AEBP2 and JARID2 (residues 140 to 166) confirm the relative localization of each of these regions in the cryo-EM map. (**D**) The JARID2 HTH (magenta) is wedged between AEBP2 (red) and the SUZ12 ABH (mint green) and NR (green).